Mustansiriyah Journal of Pure and Applied Sciences, Print ISSN: 2957-9910. Online ISSN: 2957-9929, Vol. 4, No. 3, 2026, Pages 155-170
DOI: 10.47831/mjpas.v4i3.473

MJPAS

MUSTANSIRIYAH JOURNAL OF PURE AND APPLIED SCIENCES

Journal homepage:
https://mjpas.uomustansiriyah.edu.iq/index.php/mjpas

RESEARCH ARTICLE - PHYSICS

Deoxygenation-Controlled Synthesis of ZnO Nanoparticles via Non-Thermal Plasma Jet for Optoelectronic Applications

Hussein Khalid Jasim[1], Intesar H. Hashim[1*] and Hasan A. Hadi[1]

[1]Mustansiriyah University, College of Education, Department of Physics, Baghdad-Iraq
Corresponding author: dr.intesarhato@uomustansiriyah.edu.iq

Article Info.

Article history:

Received
2 August 2025

Accepted
26 August 2025

Publishing
30 September 2026

Abstract

The present study explores the impact of oxygen reduction on the structural, electrical, and optoelectronic properties of zinc oxide nanoparticles (ZnO NPs) synthesized using non-thermal plasma jet (NTPJ), which used deionized water (DW) as the interaction medium. Four methods were used to test that. The first one was left DW without any treatment (M1). The second was DW treated with argon treatment for 10 min before use in NPs synthesis (M2). In contrast, in the third method, argon treatment was applied to DW during the entire synthesis process (M3). In the fourth one, DW was heated at 100°C and subjected to continuous argon flow during the synthesis process (M4). The characterization of zinc nanoparticles on glass and silicon was conducted using X-ray diffraction (XRD), energy-dispersive X-ray spectroscopy (EDX), and scanning electron microscopy (SEM). The EDX analysis revealed zinc: oxygen atomic ratio of 1:1, which is the stoichiometric ratio, at method M4, reducing defects and improving material properties.

The results showed highly crystalline hexagonal wurtzite of synthesized ZnO NP, with varying crystallite sizes depending on the substrate type. SEM images showed improved air permeability and aerosolization properties compared to samples with less oxygen reduction. Si/ZnO NP photodetector performance is more significant in the case of ZnO NPs synthesized in method M4, with a responsivity of 18.3 A/W and a quantum efficiency reaching nearly 40% at 330 nm wavelength.

The official journal published by the College of Education at Mustansiriyah University

Keywords: ZnO nanoparticles; SEM; EDX; NTPJ; Silicon Photodetectors

Introduction

Zinc oxide (ZnO) has a wide and direct band gap of approximately 3.3-3.4 eV at room temperature and a large exciton binding energy of 60 meV, which supports excitonic emission at or above room temperature. These properties make ZnO an auspicious material for optoelectronic applications, including UV light-emitting diodes, laser diodes, and photodetectors [1]. Also, ZnO has high radiation hardness, making it suitable for space or high-radiation environments. ZnO's wurtzite crystal structure, large piezoelectric and pyroelectric constants, and non-linear optical properties also support applications in sensors, actuators, and non-linear optical devices. High surface sensitivity to adsorbed gases, enabling its use in gas sensors and food freshness detectors [2, 3, 4], ZnO offers several advantages over other wide band gap materials by several advantages, such as the availability of bulk crystals, simpler and lower cost crystal growth technologies, Amenability to wet chemical etching, which is beneficial for device fabrication. Nanotechnology is the science and engineering of manipulating materials at the nanometer scale, typically between 1 and 100 nm. At this scale, materials exhibit unique physical, chemical, optical, and electronic properties that differ significantly from their bulk counterparts, opening new frontiers in science and technology [1, 5]. In the nano scale, ZnO NPs show a large surface area, which leads to enhanced photochemical performance and surface reactivity, and this makes it important in many applications such as UV photodetectors, gas sensors, and photocatalysis [6, 7]. Additionally, the chemical stability, low cost, and eco-friendliness

make ZnO NPs a potential material for sustainable technologies. Various techniques were used to synthesize ZnO NPs, such as sol–gel [8], hydrothermal [9], chemical precipitation [10], Among these, non-thermal plasma (also known as cold plasma) [11] has emerged as a promising technique. Nonthermal plasma in general is a partially ionized gas composed of electrons, ions, neutral particles, and photons emitted from dissociated, electrically excited molecules. It is characterized by a significant temperature difference between its energetic electrons and the relatively cold neutral species and ions. Typically generated through various electrical discharges at atmospheric pressure, non-thermal plasma exhibits minimal surface damage and a shallow penetration depth in the treated surfaces, making it especially suitable for sensitive applications such as materials surface modification, medical and agricultural fields, environmental remediation, and the synthesis of nanomaterials [12]. Among the plasma-based NP synthesis methods, non-thermal atmospheric plasma jet has gained attention due to the low-temperature treatment environment [13], high purity, support for green synthesis, and controllable particle size and morphology by adjusting plasma parameters [14,15]. Certain drawbacks must be considered when evaluating this technique, including the most significant: the uncontrolled oxidation due to plasma–liquid interactions and the large variety of reactive oxygen species (ROS) such as hydroxyl radicals (•OH), atomic oxygen (O), ozone (O_3), and hydrogen peroxide (H_2O_2) are generated through the dissociation of water molecules by energetic electrons, UV photons, or plasma-generated ions. These ROS rapidly dissolve into the surrounding liquid and initiate strong oxidation reactions with metal precursors [14, 16]. Stoichiometry in materials science refers to the precise atomic ratio between constituent elements, where each element has an activity of unity. In this ideal state, no driving force exists for atoms to leave or enter the crystal lattice, resulting in minimized defect formation and enhanced material stability [17]. For zinc oxide (ZnO), perfect stoichiometry implies a 1:1 Zn to O ratio. Deviation from this ratio, either by zinc enrichment (Zn-rich) or oxygen enrichment (O-rich), significantly influences the type and concentration of intrinsic point defects. Under Zn-rich and O-poor conditions, oxygen vacancies (V_O) tend to form more easily due to their lower formation energy, contributing to n-type conductivity but also leading to undesirable mid-gap states [1]. Conversely, in O-rich environments, the formation energy of V_O increases, reducing their presence; however, this condition favors the formation of interstitial oxygen atoms (O_i), which can occupy non-lattice positions and induce structural distortion and green-yellow photoluminescence due to deep-level transitions [1, 18]. In ZnO-based photodetectors, the stoichiometry between zinc and oxygen plays a critical role in determining device performance. When the oxygen content is initially higher than the ideal Zn:O atomic ratio of 1:1, the material typically exhibits a low concentration of oxygen vacancies (V_O), resulting in reduced photoconductive gain and limited responsivity. By applying controlled treatment parameters to minimize excess oxygen and shift the Zn: O ratio toward stoichiometry, the number of oxygen vacancies increases slightly, which can enhance photo-generated carrier separation and improve the photo response without significantly increasing the dark current. This optimized stoichiometric balance offers a trade-off between sensitivity and stability, maintaining a fast response and low noise while allowing for moderate photoconductive gain. Therefore, reaching near-stoichiometric composition in ZnO can improve the photodetector's performance by reducing deep-level defects and enabling faster, more reliable photoelectric behavior, as confirmed by recent studies [19].

Based on the critical role of stoichiometry in defining the defect structure and photoelectric behavior of ZnO NPs, this study aims to investigate the most effective method for reducing oxygen content in the water medium used during the synthesis process by a non-thermal plasma jet (NTPJ). It further examines how different substrate types influence the final oxygen percentage in the prepared ZnO NPs samples. Finally, the study aims to investigate the impact of this controlled reduction in oxygen content on the morphology and stoichiometric balance of the synthesized ZnO nanoparticles, with implications for enhancing photodetector performance through improved structural and compositional control.

Experimental part

ZnO NPs were prepared by a nonthermal plasma jet system as illustrated in Fig. 1. The plasma jet was generated using a high-voltage power supply. The high-voltage output was connected to a hollow copper electrode serving as the jet electrode, with argon gas flowing through it as the working gas. At the same time, the ground terminal was attached to a zinc rod (≥99.9%, AnalaR NORMAPUR®, VWR Chemicals, France) with dimensions of 60 mm in length × 7 mm in diameter, which functioned as the target material for nanoparticle synthesis. The copper electrode, measuring 120 mm in length, was insulated with Teflon to prevent sparking and housed inside a 140 mm long Pyrex tube with a straight nozzle configuration. The zinc rod was partially submerged in 10 mL of deionized water, serving as the reaction medium for synthesis. The plasma jet nozzle was positioned vertically at a distance of 150 mm above the water surface to ensure continuous plasma-liquid interaction. A stable plasma plume was produced at an applied voltage of 14 kV, a frequency of 8.5 kHz, and an argon flow rate of 3 L/min.

The synthesis and deposition of ZnO NPs by NTPJ were carried out at four different conditions by changing the deionized water conditions (reaction medium) as a method to reduce the oxygen ratio of the resulting ZnO NPs. These conditions involved treating four samples of DW using different conditions. The first sample was left without any treatment (M1). In contrast, the rest of the samples were treated respectively with argon treatment for 10 min before use in NPs synthesis (M2), argon treatment during the entire synthesis process (M3), and heating DW at 100°C and subjecting it to continuous argon flow during synthesis process (M4). For all cases, the zinc materials were immersed in DW and used as the target for ZnO NPs preparation.

The resulting ZnO NPs prepared using NTPJ by aiding untreated and treated DW with different treatment methods were deposited onto glass using the drop-casting method. Before deposition, the substrates were previously cleaned in ethanol and deionized water for 5 minutes each using an ultrasonic cleaner, followed by hot air drying. A 2 mL aliquot of the ZnO NP solution was then dispensed onto glass using a micropipette. Finally, the deposited samples were dried at RT for 24 hours.

The prepared ZnO NPs at the best treatment condition (heating DW at 100°C and subjecting it to continuous argon flow during preparation) were used to deposit them on silicon substrates p-Si (100) (Si_{M4}), to build ZnO NPs/Si photodetectors, and then to compare them with that of ZnO NPs/Si photodetectors prepared at untreated DW (Si_{M1}). The same cleaning and deposition conditions used for the glass substrates were applied to the silicon substrates.

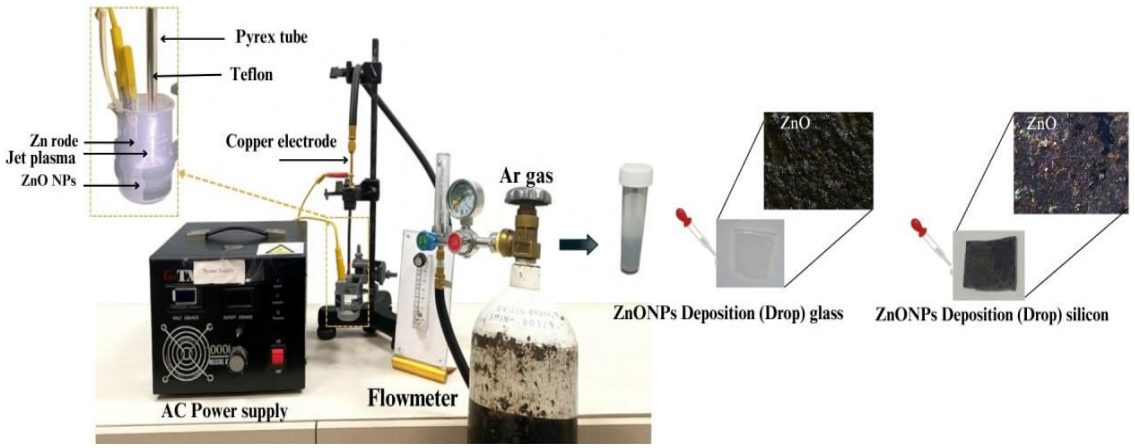

Figure 1: Experimental schematic of ZnO NPs preparation by NTPJ

The crystalline structure of ZnO NPs was examined using X-ray diffraction (XRD) (PANalytical Aeris) with Cu Kα radiation ($\lambda = 1.5406$ Å). The surface morphology and elemental composition were studied by Dispersive Energy (EDX) with the Axia Chemi SEM in conjunction with SEM.

Dark/photo-current-voltage (I-V) characteristics were examined using a DC digital power supply (YAXUN PS - 1502DD), a multimeter (Pros Kit MT-1132), and a 150 W halogen light source. The photodetector characteristics were obtained by using a digital Mini-Chrome (DMC1-03 from Optometric Corporation /USA 300 nm to 800 nm), an Halogen spectral lamp (Phywe / Germany); laser power meter LP1 (sawn/Japan) was employed for power calibration.

Results and discussion

EDX analysis

Energy dispersive X-ray spectroscopy (EDX) was employed to investigate the effectiveness of the method used to reduce the oxygen content during the synthesis of ZnO nanoparticles (ZnO NPs) by chemical characterization and analyzing the elemental composition of the resulting nanoparticles, which enabled a direct comparison of the oxygen and zinc percentages. The deviations from stoichiometry in each method were evaluated by comparing the Zn to O atomic ratio to the ideal stoichiometric ratio of ZnO. Fig. 2 illustrates the EDX spectrum for ZnO NPs synthesized by NTPJ at synthesis duration of 15 min, an applied voltage of 14 kV, and a flow rate of 3 L/min. The sample synthesis without treated DW exhibited a Zn:O atomic ratio of 1:10, indicating a significant deviation from the ideal stoichiometric ratio. After applying the oxygen-reduced methods, which include treating DW with 10 min of argon before use in ZnO NP synthesis, treating DW with argon during the entire ZnO NP synthesis time, and heating DW before use to 100°C and applying argon gas during the preparation process as a whole, the EDX spectrum revealed a noticeable decrease in the Zn:O atomic ratio to a more balanced ratio of 1:7, 1:2, and 1:1, respectively. This indicates a reduction in oxygen percentage and a shift to stoichiometry. At the same time, the zinc content increased proportionally. In the three oxygen-reduction methods applied, two key parameters were responsible for decreasing the oxygen percentage in the ZnO samples: heating and the use of argon gas. These parameters, either individually or in combination, contributed to the removal of dissolved oxygen (DO) species from the ZnO surface, as confirmed by EDX analysis. According to Henry Low, the decrease in DO after heating is due to the heating leading to a reduction in the solubility of the gases due to the gas and molecular water gaining more energy and breaking intermolecular bonds between the oxygen solute and water [20, 21]. The second parameter is introducing the argon gas into DW. Argon is an inert gas and does not chemically interact with water or zinc; instead, it displaces dissolved oxygen by physically sweeping oxygen molecules out of the liquid. This process is called gas purging or deaeration [22, 23]. From the methods used to reduce the DO, the combination of argon bubbling and heating showed the most effective results. This method led to the lowest oxygen percentage in the ZnO samples, as confirmed by EDX analysis, indicating that the simultaneous removal of dissolved oxygen by argon and thermal desorption significantly enhances oxygen reduction efficiency. The element percentage for all prepared samples is summarized in Fig. 3 and Table 1. In Table 1, the atomic and weight ratios of Zn and O, in addition to the ZnO:O ratio, are illustrated.

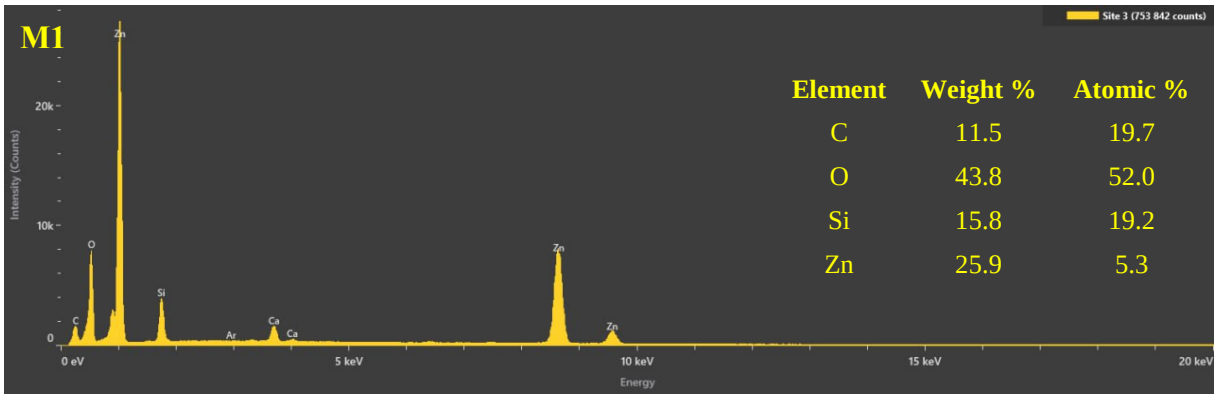

Element	Weight %	Atomic %
C	11.5	19.7
O	43.8	52.0
Si	15.8	19.2
Zn	25.9	5.3

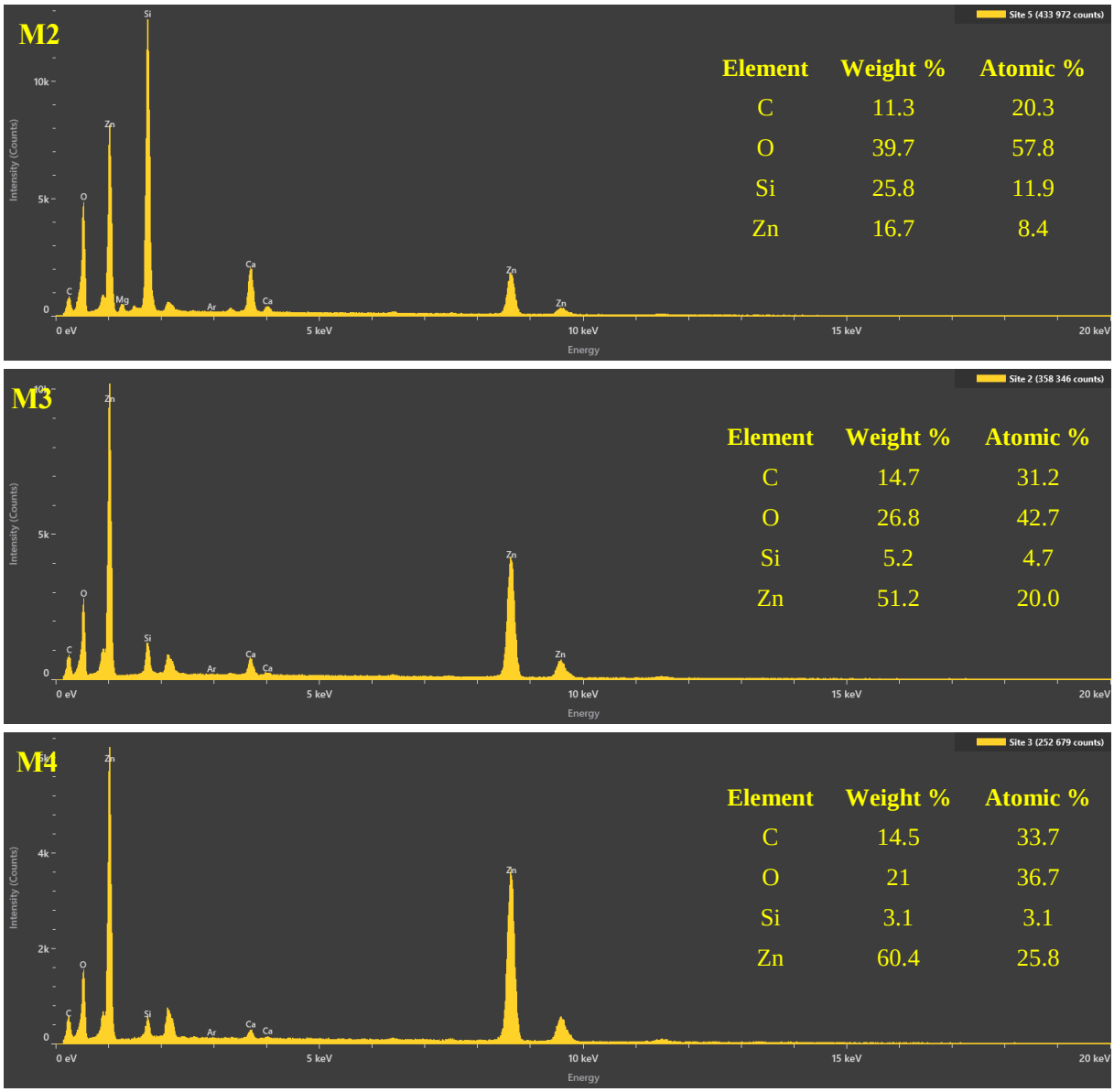

Figure 2: EDX spectra distribution and data of elements percentage for ZnO NPs deposited on a glass substrate, synthesized by NTPJ for 15 min, using different methods to reduce oxygen percentage (M1, M2, M3, and M4).

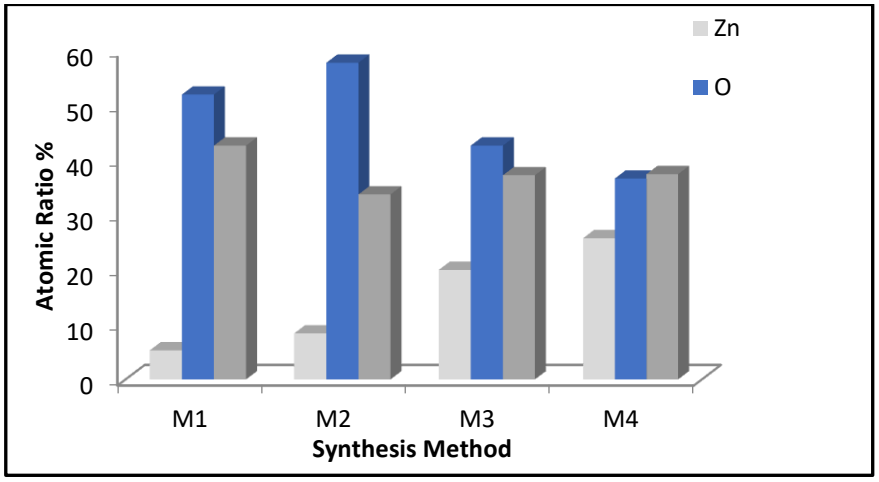

Figure 3: Elements percentage for ZnO NPs deposited on a glass substrate, synthesized by NTPJ for 15 min, using different methods to reduce oxygen percentage (M1, M2, M3, and M4).

Table 1: Element percentage in ZnO NPs samples, deposited on a glass substrate, synthesized by NTPJ for 15 min, using different methods to reduce oxygen percentage

Method	Weight %		Atomic %		Zn:O Weight ratio	Zn:O Atomic ratio	
	Zn	O	Zn	O			
M1	25.9	43.8	5.3	52.0	0.591	0.1	~1:10
M2	16.7	39.7	8.4	57.8	1.52	0.145	~1:7
M3	51.2	26.8	20.0	42.7	1.91	0.468	~1:2
M4	60.4	21	25.8	36.7	2.87	0.7	~1:1

Based on EDX results, the best method for reducing oxygen was M4 (heating DW at 100°C and subjecting it to continuous argon flow during the synthesis process). ZnO NPs synthesized using the M4 method were deposited on p-Si (100) substrates to investigate how the substrate material influences oxygen percentage and compare with that deposited using ZnO NPs synthesized using the M1 method. Fig. 4 shows the EDX spectra of these two samples. The results illustrate that the oxygen percentage using the M4 method was lower than that using the M1 method, approaching the stoichiometry of ZnO (1:1). Furthermore, when compared to a glass substrate, the glass shows a significantly higher oxygen signal. This can be attributed to both increased ZnO NP loading and additional oxygen contributions from the SiO_2-based glass. In contrast, the silicon substrate exhibits a relatively lower oxygen percentage, likely due to reduced surface retention and minimal oxygen content from the substrate itself. The element percentage for all prepared samples is summarized in Fig. 5 and Table 2.

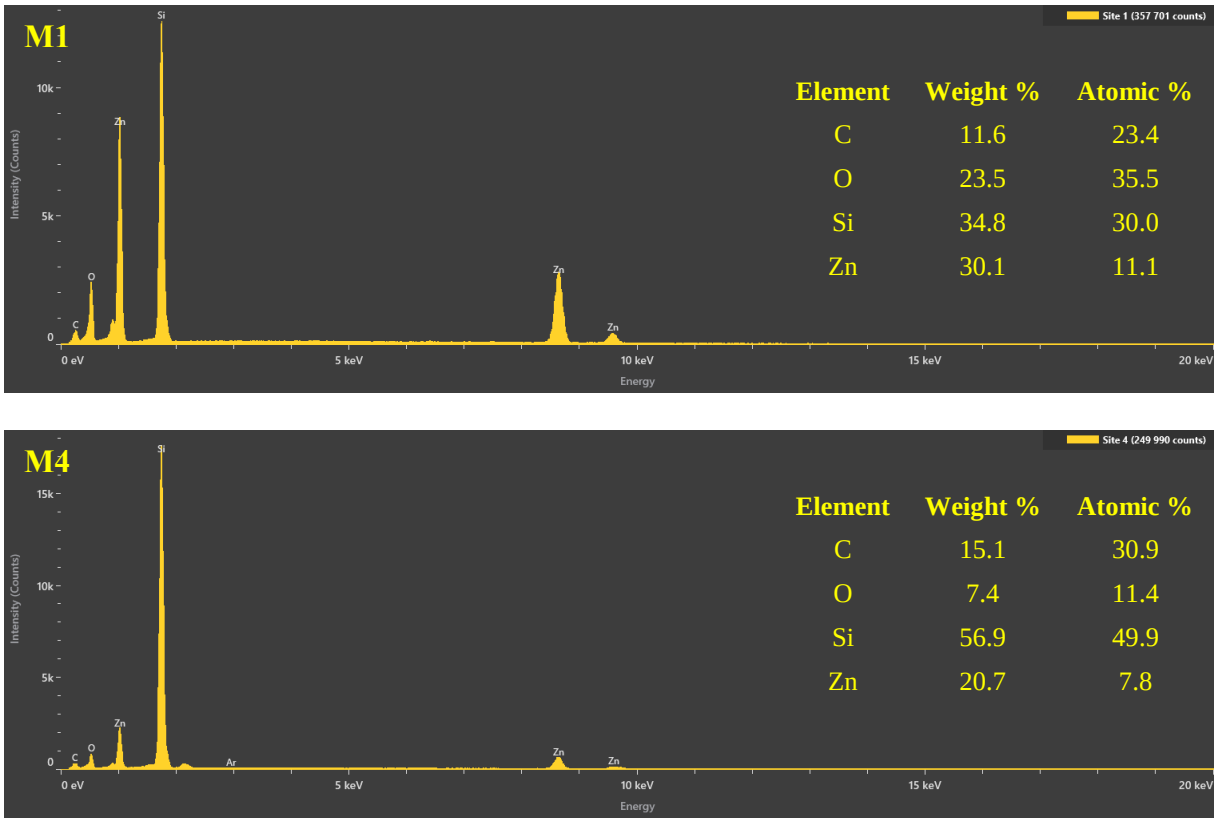

Figure 4: EDX spectra distribution and data of elements percentage for ZnO NPs deposited on a silicon substrate, synthesized by NTPJ for 15 min, using different methods to reduce oxygen percentage (M1 and M4).

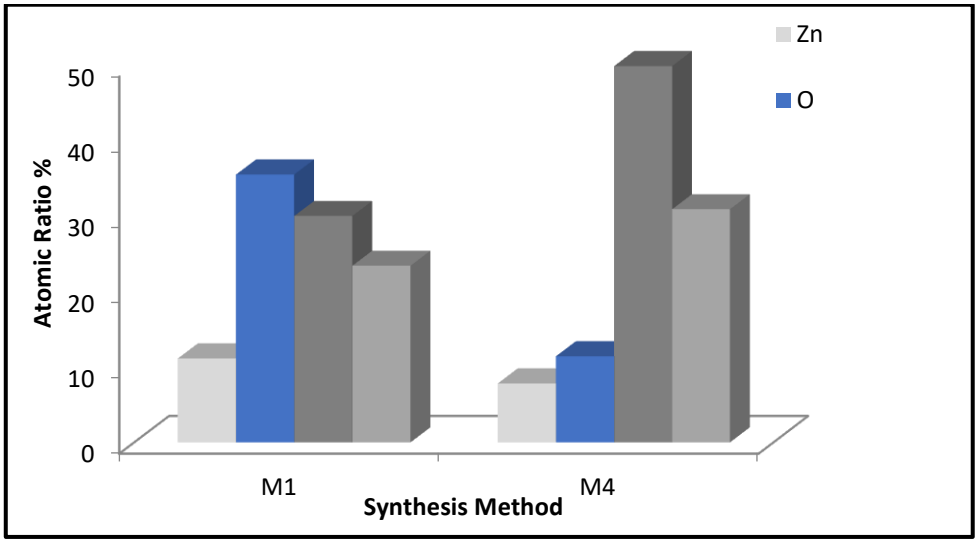

Figure 5: Elements percentage of ZnO NPs deposited on a silicon substrate, synthesized by NTPJ for 15 min, using different methods to reduce oxygen percentage (M1 and M4).

Table 2: Element percentage in ZnO NPs samples, deposited on a silicon substrate, synthesized by NTPJ for 15 min, using different methods to reduce oxygen percentage

Method	Weight %		Atomic %		Zn:O Weight ratio	Zn:O Atomic ratio	
	Zn	O	Zn	O			
M1	30.1	23.5	11.1	35.5	1.28	0.312	~1:3
M4	20.7	7.4	7.8	11.4	2.79	0.68	~1:1

SEM analysis

Fig. 6 shows the morphology of ZnO NPs samples prepared using different oxygen-reducing methods and deposited on a silicon substrate. The SEM images illustrate that the morphology of ZnO NPs was significantly influenced by the treatment conditions of the deionized water (DW) used during synthesis via non-thermal atmospheric argon plasma jet. The untreated DW sample (M1) exhibited irregular and densely packed nanoparticles with high agglomeration. The sample prepared with DW treated with argon gas for 10 minutes before preparation (M2) showed more uniform and spherical nanoparticles with improved dispersion. Meanwhile, the sample prepared by DW was treated with argon during the entire synthesis process (M3) and presented large, plate-like, or bulk structures. Additionally, the sample morphology that was prepared with heating DW before preparation to 100°C and applying argon gas during the entire preparation process (M4) demonstrated compact, granular nanoparticles with relatively uniform morphology, with a change in shape tending to be sheet-like. Non-thermal plasma can transform granular/spherical ZnO NPs into plate-like, rod-like, or sheet-like morphologies by controlling nucleation, growth rates, surface passivation, and oriented attachment [24]. These results confirm that the treatment of deionized water plays a critical role in maintaining the morphology, size, and distribution of ZnO nanoparticles during plasma-assisted synthesis.

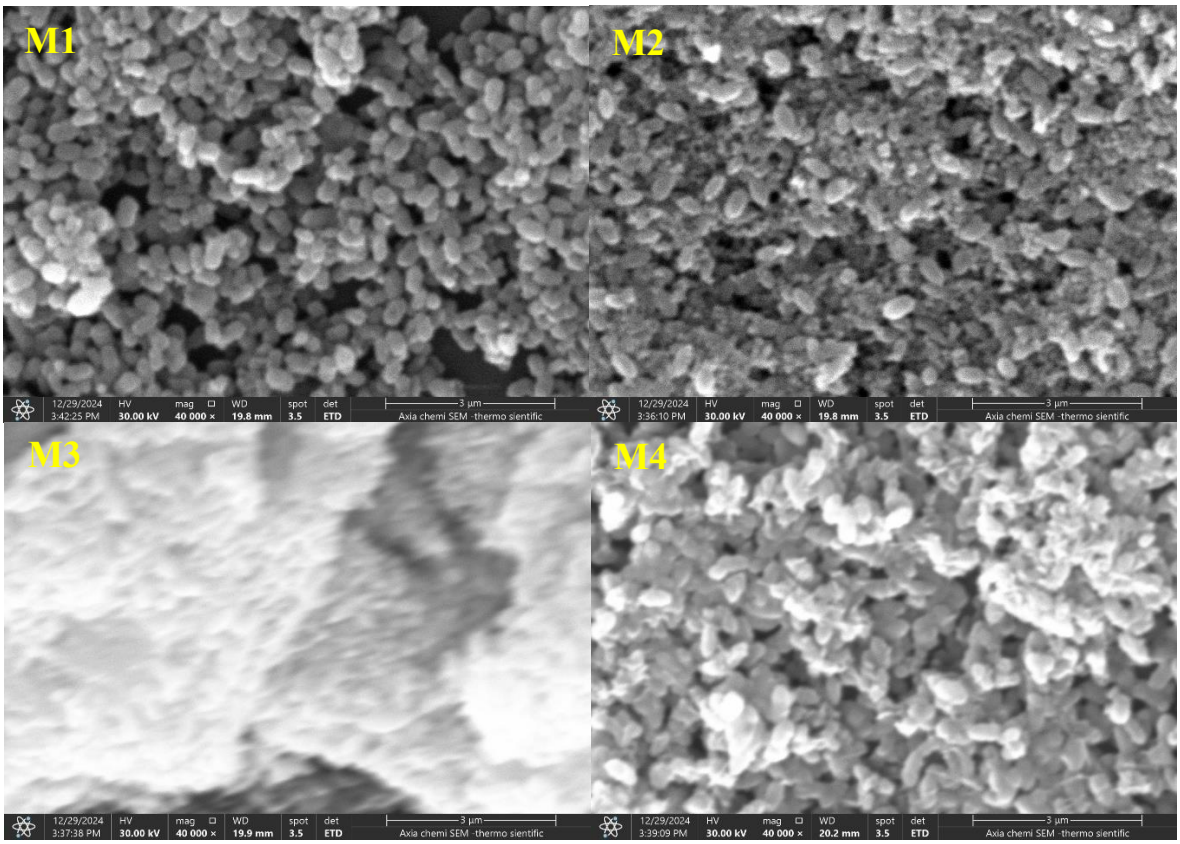

Figure 6*:* SEM for ZnO NPs deposited on a glass substrate, synthesized by NTPJ for 15 min, using different methods to reduce oxygen percentage (M1, M2, M3, and M4).

The morphology of ZnO NP samples prepared by untreated DW (M1) and DW treated with heating to 100°C before preparation and applying argon gas during the entire preparation process (M4) is illustrated in Fig. 7. The image of M1 shows that the ZnO NPs surface exhibits large, irregular agglomerates with a rough and uneven texture. In contrast, image M4 displays a much smoother and more homogeneous surface morphology. The ZnO NPs appear to be well-dispersed with minimal visible agglomerates. These observations confirm that the preparation conditions are effective in refining the morphology of ZnO NPs, making them more suitable for applications that require uniform surface coverage and high surface activity.

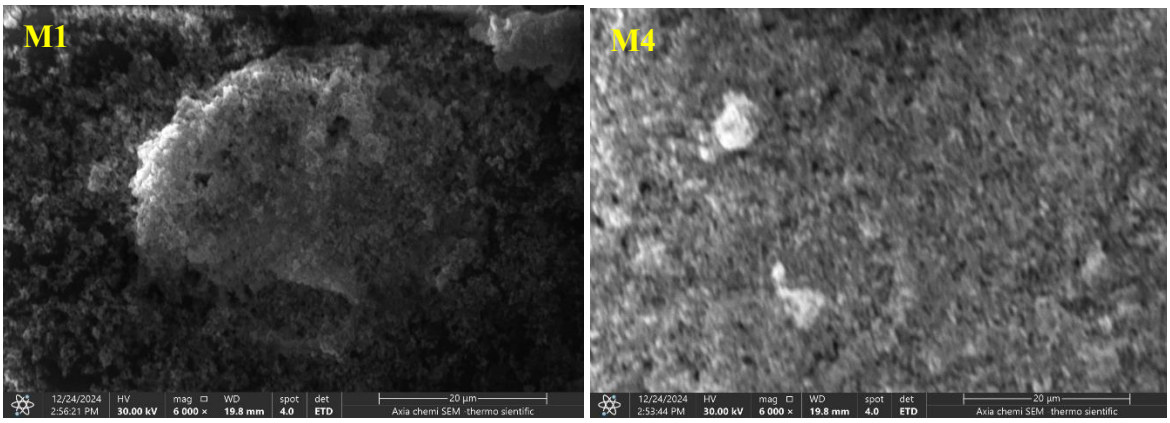

Figure 7: SEM for ZnO NPs samples deposited on a silicon substrate, synthesized by NTPJ for 15 min, using different methods to reduce oxygen percentage (M1 and M4).

XRD analysis

Fig. 8 illustrates the XRD patterns of ZnO NPs prepared by NTPJ in M4 (the most effective method for reducing the oxygen percentage, as ensured by experimental results) and deposited on glass and silicon to investigate the crystalline structure and determine the crystallite size of the resulting thin films. The XRD pattern shows characteristic peaks at $2\theta = 33.6°$, 35°, and 36.8°, corresponding to the (100), (002), (101), and (102) planes, and at $2\theta = 33.6°$ and 63.3°, corresponding to the (100) and (103) planes of the hexagonal wurtzite structure of ZnO NPs (JCPDS card no. 96-230-0116), deposited on glass and silicon, respectively. The sharp and intense diffraction peaks confirm the high crystallinity of the sample. The average crystallite size (D) was estimated using the Scherrer equation [25]:

$$D = \frac{K\lambda}{FWHM * \cos\theta} \qquad (1)$$

where D denotes the crystallite size of the ZnO NPs, FWHM refers to the full width at half maximum of the diffraction peak, K is the Scherrer constant, θ is the Bragg diffraction angle, and λ represents the wavelength of the Cu $K\alpha_1$ radiation.

The calculated average crystallite size was found to be approximately 10.6 nm and 70 nm for ZnO NPs deposited on glass and silicon, respectively. The obtained results confirm the nanostructured nature of the ZnO Nps thin film, showing that ZnO NPs deposited on glass have a smaller crystallite size compared to ZnO NPs deposited on silicon. This can be attributed to the structured lattice of Si(100), which provides a template that reduces randomized nucleation, allowing larger grains and higher crystal orientation relative to the amorphous glass surface [26].

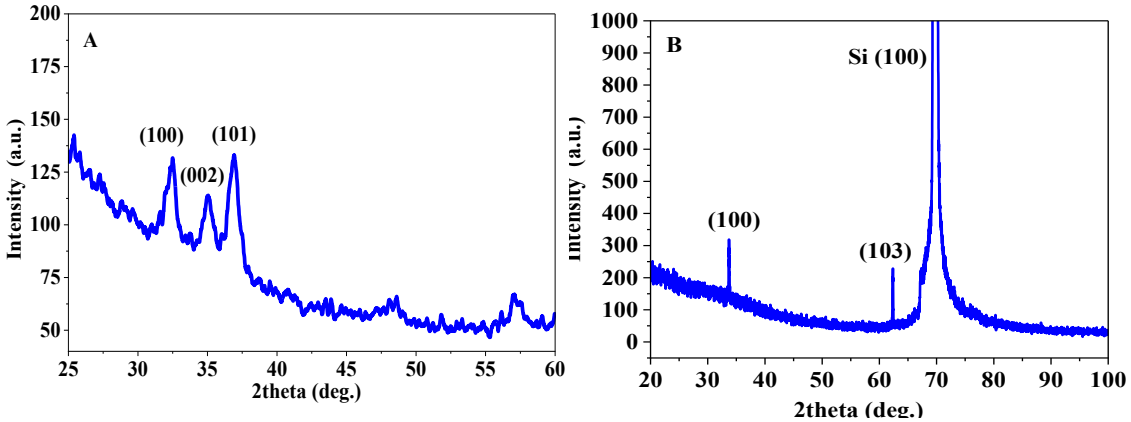

Figure 8: XRD pattern of ZnO NPs samples synthesized by NTPJ for 15 min, using M4 method to reduce oxygen percentage, A) deposited on a glass substrate, B) deposited on a silicon substrate.

Electrical properties

To illustrate the effectiveness of the method M4, as the best reduced oxygen method, on the electrical properties of ZnO NP synthesis by it, and compare with the properties of that synthesized using M1. The current–voltage (I–V) characteristics of the Si/ZnO NPs devices, as shown in Fig. 9, display apparent differences in electrical behavior between samples M1 and M4. Sample M1, which contains a higher oxygen percentage, exhibits a lower current response compared to M4 across the measured voltage range. This reduced conductivity is attributed to the dominance of interstitial oxygen defects (O_i) in M1, which act as deep-level recombination centers, trapping charge carriers and suppressing electron mobility [18]. In contrast, M4, being relatively oxygen-deficient, likely contains a higher concentration of oxygen vacancies (V_O), which serve as shallow donors and enhance n-type conductivity by supplying free electrons to the conduction band [26, 27].

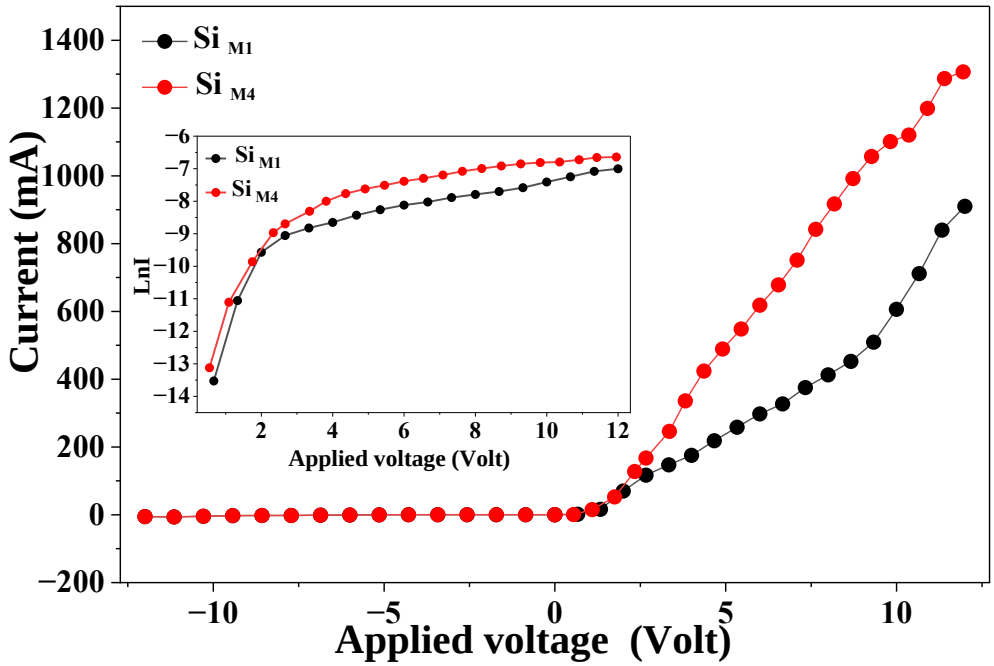

Figure 9: Dark I-V characteristic of ZnO nanoparticles deposited on a silicon substrate, Si_{M1} and Si_{M4}, with inset (Semi-logarithmic I-V plot)

The ideality factor, saturation current, and barrier height were extracted using the standard diode equation [29]:

$$I=I_s\left[\exp\left(\frac{qV}{nkT}\right)-1\right] \qquad (2)$$

where q is elementary charge, T is the absolute temperature in Kelvin, k is the Boltzmann constant, V is the applied voltage, and I_s denotes the reverse saturation current.

The Schottky barrier $\emptyset_b$ height was determined using the following relation:

$$\emptyset_b=\frac{kT}{q}\ln\left(AA^*\frac{T^2}{I_s}\right) \qquad (3)$$

where, A is the diode area, and A*is the Richardson constant, taken as 32 A cm^{-2} K^{-2} for p-Si type, Additionally, the saturation current can also be described by:

$$I_s=AA^*T^2\exp\left(\frac{-q\,\emptyset_b}{nkT}\right) \qquad (4)$$

The ideality factor, which was derived from the slope of the linear region of forward bias (ln I - V) through the equation

$$n=\frac{q}{kT}\left(\frac{dV}{d\ln I}\right) \qquad (5)$$

The reverse bias saturation current, a key diode parameter, was determined by analyzing the semi-logarithmic linear region of the current–voltage (I–V) curve, as depicted in the inset of Fig. 9.
The extracted electrical parameters show that the saturation current (Is) for M1 is 2.1×10^{-7}A, while M4 reaches 5.6×10^{-7}A, indicating improved electron injection in the latter. The ideality factor (n) decreases from 2.3 in the M1 to 1.8 in the M4, suggesting a closer approach to ideal diode behavior and reduced defect-assisted transport. The Schottky barrier height $\emptyset_b$ slightly decreases from 0.80 V to 0.78 V, consistent with enhanced carrier transport under reduced oxygen conditions. Interestingly, the forward resistance (R_f) at 3 V increases from 736 in M1 to 819 in M4, indicating that oxygen reduction improves charge separation and reduces recombination. Overall, these findings demonstrate that tuning

oxygen content toward stoichiometry can significantly enhance ZnO electrical performance by balancing conductivity, recombination suppression, and diode quality [18, 27, 28].

Fig. 10 illustrates illuminated (I-V) characteristics of ZnO NPs /p-Si for both samples. The electrical behavior was examined by recording current–voltage characteristics under increasing halogen illumination intensity of 50, 100, and 150 mW/cm². The M4 sample has stronger photocurrent response compared to M1. This enhancement arises because moderate oxygen deficiency introduces oxygen vacancies (V_O) that act as shallow donor states, increasing carrier concentration and improving conductivity under light exposure. At the same time, a too-high oxygen concentration (as in Si_{M1}) may reduce V_O levels and lead to surface oxygen species or interstitial defects that increase recombination and limit photocurrent (moderately oxygen-deficient samples tend to show optimal performance) [30, 31]. Previous studies confirm that carefully controlled oxygen vacancy concentrations in ZnO nanoparticles significantly enhance photoconductive performance, whereas either extremes, high vacancy concentrations (which slow response) or very low vacancy levels (which lower photocurrent), are suboptimal [29].

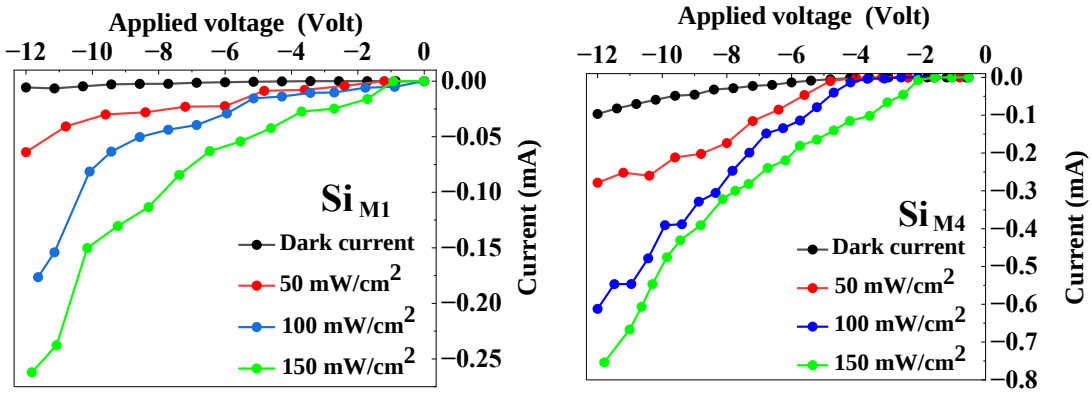

Figure 10: Illuminated I-V characteristic of ZnO nanoparticles deposited on a silicon substrate, Si_{M1} and Si_{M4} sample

Figure of merit of photodetector

To investigate the effectiveness of the best oxygen reduction method, found from the results, on the optoelectronic performance of ZnO NPs/Si photodetectors, the key figure of merit, including responsivity, external quantum efficiency, and detectivity, was analyzed.

Responsivity is defined as the ratio of output photocurrent to incident optical power (A/W) [32]:

$$R_\lambda = \frac{I_{ph}}{P_{in}} \qquad (6)$$

where I_{ph} is photocurrent and P_{in} incident power.

External quantum efficiency is defined as the ratio of the number of collected electron–hole pairs to the number of incident photons [33]:

$$EQE = \frac{1240\, R_\lambda}{\lambda nm} \qquad (7)$$

where R_λ is the responsivity and λ is the wavelength of an incident photon.

Detectivity, which reflects the photodetector's ability to detect weak signals in the presence of noise, was elevated as the dark current remained relatively low despite the improved photocurrent [34]:

$$D^* = \frac{R_\lambda \sqrt{A}}{\sqrt{2qI_d}} \qquad (8)$$

where A represent the active area of the detector, q electron charge, I_d dark current.

Fig. 11a, b, and c show the responsivity, external quantum efficiency, and detectivity of samples M1 and M4 as functions of wavelength in the 200 to 800 nm range at a -5 V bias. The spectra for all three

figures of merit display three emission peaks. The first peak appears at 330 nm, which is attributed to the bandgap absorption of ZnO. Due to quantum size effects or defects in ZnO NPs, this peak can shift slightly toward lower wavelengths (blue-shifted) [35, 36]. The second peak at 510 nm is attributed to deep-level defect transitions within the ZnO nanoparticles, specifically those associated with oxygen vacancies (V_O) [37, 38]**.** Additionally, Near-infrared emission at 730 nm is attributed to absorption by the Si substrate [39].

The enhancement in responsivity in method M4 reached 18.3 A/W confirming more efficient light-to-current conversion, while the higher EQE reached near 40% indicating improved carrier generation and collection efficiency. Furthermore, the detectivity of M4 reflects greater sensitivity and lower noise levels under weak light conditions, reaching $16710^{11}\ W^{-1}cm.Hz^{1/2}$. This improvement is attributed to the increased density of oxygen vacancies (V_O) in M4, which act as shallow donors, boosting free electron concentration and enhancing conductivity and photocurrent gain [40]. The results are summarized in Table 3.

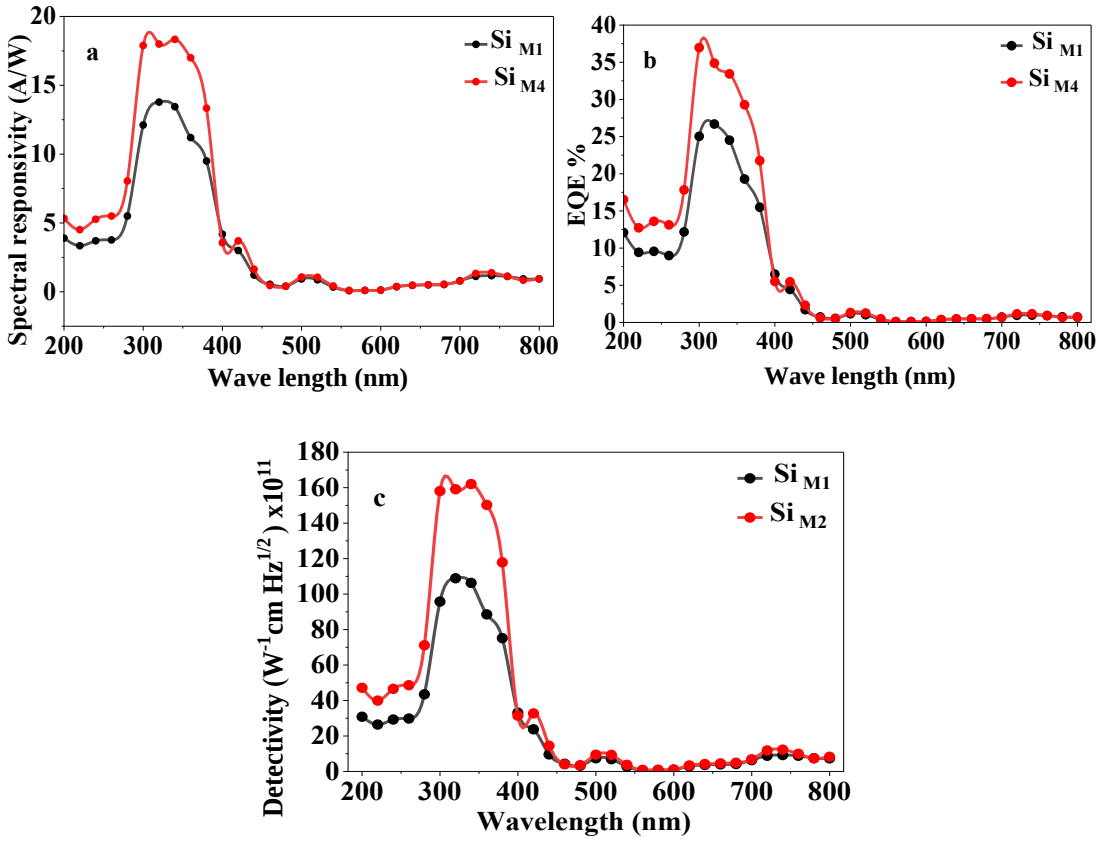

Figure 11: a) Responsivity, b) Quantum efficiency, c) Detectivity as a function of incident wavelength for ZnO nanoparticles deposited on a silicon substrate, Si_{M1}, and Si_{M4} sample at -5V bias

Table 2: Summarize the figures of merit for ZnO nanoparticles deposited on a silicon substrate, Si_{M1} and Si_{M2} sample, at -5V bias

Samples	**Responsivity** R_λ (A/W)			**Quantum Efficiency EQE (%)**			**Specific Detectivity** $(W^{-1}cm.Hz^{1/2}) \times 10^{11}$		
	330 nm	**510 nm**	**730 nm**	**330 nm**	**510 nm**	**730 nm**	**330 nm**	**510 nm**	**730 nm**
Si_{M1}	13.7	0.8	1	27	1.4	1	110	8.1	9
Si_{M4}	18.3	0.9	1.4	38	1.5	1.3	167	10.8	13

Conclusion

The study found that controlling oxygen content during the preparation of zinc oxide nanoparticles using a non-thermal plasma jet significantly impacts their properties. The most effective method was heating deionized water to 100°C with continuous argon gas flow, which reduced excess oxygen. This method was employed to improve the conductivity and enhance the performance of the Si/ZnO NPs photodetector. Oxygen reduction in oxide nanoparticles often involves removing oxygen atoms, leaving behind oxygen vacancies ($\mathbf{V_o}$). These vacancies act as n-type dopants, donating electrons to the conduction band. More free carriers lead to faster photoresponse in photodetectors, which agrees with [18]. The optimized sample also achieved a higher photocurrent response of 18.3 A/W and an external quantum efficiency of 38% at a -5 V bias voltage and 330 nm. This study suggests that precise oxygen control during ZnO preparation is an effective strategy for improving material performance in optoelectronic applications.

Acknowledgement

The authors thank Mustansiryiah University –Iraq for their logistical support.

References

[1] A. Janotti and C. G. Van De Walle, “Fundamentals of zinc oxide as a semiconductor,” Rep. Prog. Phys., vol. 72, no. 12, pp. 126501, 2009, doi: 10.1088/0034-4885/72/12/126501.

[2] O. Schmidt, P. Kiesel, C. G. Van de Walle, N. M. Johnson, J. Nause, and G. H. Döhler, “Effects of an electrically conducting layer at the zinc oxide surface,” Jpn. J. Appl. Phys., vol. 44, no. 10R, pp. 7271, 2005.

[3] O. Schmidt et al., “Analysis of a conducting channel at the native zinc oxide surface,” Superlattices Microstruct., vol. 39, no. 1–4, pp. 8–16, 2006.

[4] D. C. Look, “Quantitative analysis of surface donors in ZnO,” Surf. Sci., vol. 601, no. 23, pp. 5315–5319, 2007.

[5] I. H. Hashim, Z. S. Mahdi, and N. M. Jassim, “Bactericidal effects of silver nanoparticles prepared by green synthesis,” Mustansiriyah J. Pure Appl. Sci., vol. 2, no. 4, pp. 1–6, 2024.

[6] S. Baruah and J. Dutta, “Hydrothermal growth of ZnO nanostructures,” Sci. Technol. Adv. Mater., vol. 10, no. 1, p. 013001, 2009.

[7] Z. L. Wang, “Zinc oxide nanostructures: growth, properties and applications,” J. Phys. Condens. Matter, vol. 16, no. 25, pp. R829, 2004.

[8] T. D. H. Le and K. S. Trinh, “Synthesis of zinc oxide nanoparticles and their antibacterial activity,” in Proc. 2020 5th Int. Conf. Green Technol. Sustain. Dev. (GTSD), IEEE, 2020, pp. 119–123.

[9] H. Wei, Y. Wu, N. Lun, and C. Hu, “Hydrothermal synthesis and characterization of ZnO nanorods,” Mater. Sci. Eng. A, vol. 393, no. 1–2, pp. 80–82, 2005.

[10] A. Saka, L. Tesfaye, and K. Ramaswamy, “Synthesis, characterization, and applications of ZnO, Ag_2O, and ZnO/Ag_2O nanocomposites: A review,” Adv. Condens. Matter Phys., vol. 2024, no. 1, pp. 5755167, 2024.

[11] G. Primc, K. Brenčič, M. Mozetič, and M. Gorjanc, “Recent advances in the plasma-assisted synthesis of zinc oxide nanoparticles,” Nanomaterials, vol. 11, no. 5, pp. 1191, 2021.

[12] H. G. Hassan and I. H. Hashim, “Study of the effect of DBD plasma performance by changing the electrode configuration,” Mustansiriyah J. Pure Appl. Sci., vol. 3, no. 2, pp. 104–112, 2025.

[13] I. H. Hashim, H. A. Hadi, and N. D. H. Hayif, "Non-thermal atmospheric jet plasma effects on the morphological, electrical and optical properties of nanocrystalline silicon," Mustansiriyah J. Pure Appl. Sci., vol. 2, no. 4, pp. 93–103, 2024.

[14] Q. Chen, J. Li, and Y. Li, "A review of plasma-liquid interactions for nanomaterial synthesis," J. Phys. D: Appl. Phys., vol. 48, no. 42, pp. 424005, 2015, doi: 10.1088/0022-3727/48/42/424005.

[15] R. S. Mohammed, A. Sudhakaran, M. Y. A. Mostafa, and G. Abbady, "Synthesize of ZnO and CuO nanoparticles with plasma jet at different treatment times and testing its optical parameters with UV-Vis-NIR," Appl. Phys. A, vol. 130, no. 8, pp. 533, 2024, doi: 10.1007/s00339-024-07651-z.

[16] V. P. Thai, T. N. Dam, K. Takahashi, T. Sasaki, and T. Kikuchi, "The generation pathways of OH and H_2O_2 by plasma-liquid interactions," in IOP Conf. Ser.: Earth Environ. Sci., vol. 120, pp. 012030, 2023.

[17] C. Nicollet and A. J. Carrillo, "Back to basics: synthesis of metal oxides," J. Electroceram., vol. 52, no. 1, pp. 10–28, 2024.

[18] A. Sahai and N. Goswami, "Probing the dominance of interstitial oxygen defects in ZnO nanoparticles through structural and optical characterizations," Ceram. Int., vol. 40, no. 9, pp. 14569–14578, 2014.

[19] H. Ma et al., "Effect of surface oxygen vacancy defects on the performance of ZnO quantum dots ultraviolet photodetector," Chin. Phys. B, vol. 30, no. 8, pp. 087303, 2021.

[20] L. Li, H. Nakajima, and K. Ito, "Boiling effect on oxygen evolution reaction-Theoretical analysis of its mass transfer enhancement mechanism," Int. J. Hydrogen Energy, vol. 49, pp. 533–552, 2024.

[21] T. R. Rettich, R. Battino, and E. Wilhelm, "Solubility of gases in liquids. 22. High-precision determination of Henry's law constants of oxygen in liquid water from T = 274 K to T = 328 K," J. Chem. Thermodyn., vol. 32, no. 9, pp. 1145–1156, 2000.

[22] R. del Barrio-Galán, I. Nevares, S. Pérez-Magariño, and M. del Alamo-Sanza, "Dissolved oxygen removal in wines by gas sparging, its optimization and chemical impact," Beverages, vol. 10, no. 1, pp. 3, 2023.

[23] K. Park and M. Catalfomo, "Gas chromatographic determination of dissolved oxygen in sea water using argon as carrier gas," in Deep Sea Res. Oceanogr. Abstr., Elsevier, 1964, pp. 917–920.

[24] H. Mohan, S. Mohandoss, N. Balasubramaniyan, & S. Loganathan, "Non-Thermal Plasma-Assisted Synthesis of ZnO for Enhanced Photocatalytic Performance". *Plasma*, vol. *8*, no.2), pp. 25. 2025.

[25] A. S. Abdulhameed, H. A. Hadi, and R. A. Ismail, "New trends in the preparation of high-performance Au/B-Si photodetector by wet chemical etching: the effect of etching time," J. Mater. Sci. Mater. Electron. vol. 35, no. 10, pp. 1–18, 2024.

[26] A. Taabouche et al., "Effect of substrates on the properties of ZnO thin films grown by pulsed laser deposition," Adv. Mater. Phys. Chem., vol. 2013, 2013.

[27] A. Janotti and C. G. Van de Walle, "Native point defects in ZnO," Phys. Rev. B, vol. 76, no. 16, pp. 165202, 2007.

[28] A. Kołodziejczak-Radzimska and T. Jesionowski, "Zinc oxide—from synthesis to application: a review," Materials (Basel), vol. 7, no. 4, pp. 2833–2881, 2014.

[29] A. S. Abdulhameed, H. A. Hadi, and R. A. Ismail, "Structural and optical properties of black silicon prepared by wet chemical etching," Mustansiriyah J. Pure Appl. Sci., vol. 3, no. 1, pp. 123–134, 2025.

[30] C. Ling et al., "Oxygen vacancies enhanced photoresponsive performance of ZnO nanoparticles thin film/Si heterojunctions for ultraviolet/infrared photodetector," J. Alloys Compd., vol. 797, pp. 1224–1231, 2019.

[31] Y. Kang, H.-H. Nahm, and S. Han, "Light-induced peroxide formation in ZnO: Origin of persistent photoconductivity," Sci. Rep., vol. 6, pp. 35148, 2016.

[32] H. A. Hadi, "Fabrication, morphological and optoelectronic properties of antimony on porous silicon as MSM photodetector," J. Fundam. Appl. Sci., vol. 6, no. 2, pp. 175–186, 2014.

[33] N. D. Hayif, H. A. Hadi, and I. H. Hashim, "Effect of applied voltage on the properties of non-thermal DBD plasma used to enhance porous silicon/n-Si heterojunction photodetector performance," J. Opt., pp. 1–11, 2024, doi: 10.1007/s12596-024-02105-4.

[34] N. D. Hayif, H. A. Hadi, and I. H. Hashim, "Enhancement of performance Au/PSi/n-Si/Ag heterojunction photodetector by non-thermal plasma jet: Design and impact of plasma voltage," Silicon, vol. 17, no. 3, pp. 531–554, 2025.

[35] Z. Cao, Y. Wang, Z. Li, and N. Yu, "Hydrothermal synthesis of ZnO structures formed by high-aspect-ratio nanowires for acetone detection," Nanoscale Res. Lett., vol. 11, pp. 1–6, 2016.

[36] Ü. Özgür et al., "A comprehensive review of ZnO materials and devices," J. Appl. Phys., vol. 98, no. 4, pp. 041301, 2005, doi: 10.1063/1.1992666.

[37] K. Vanheusden, C. H. Seager, W. L. Warren, D. R. Tallant, and J. A. Voigt, "Correlation between photoluminescence and oxygen vacancies in ZnO phosphors," Appl. Phys. Lett., vol. 68, no. 3, pp. 403–405, 1996.

[38] K. Vanheusden et al., "Green photoluminescence efficiency and free-carrier density in ZnO phosphor powders prepared by spray pyrolysis," J. Lumin., vol. 75, no. 1, pp. 11–16, 1997.

[39] S. S. Kurbanov, G. N. Panin, T. W. Kim, and T. W. Kang, "Strong violet luminescence from ZnO nanocrystals grown by the low-temperature chemical solution deposition," J. Lumin., vol. 129, no. 9, pp. 1099–1104, 2009.

[40] L. Liu et al., "Oxygen vacancies: The origin of n-type conductivity in ZnO," Phys. Rev. B, vol. 93, no. 23, pp. 235305, 2016.